where q_e is the electron charge. This is because their diffusion through a distance r 'flips' water dipoles over their entire path, creating a total dipole field change of $\pm(0.38\,q_e)r$ (ref. 1). Thus a D defect reduces the field by 0.38 of the initial value as they traverse the film. Only D defects move; the field polarity keeps any negative-like L defects at the film top.

Figure 3 shows the shapes of the ΔV versus T curves for a variety of field strengths, $(1.1–11) \times 10^7\,V\,m^{-1}$. These fields are weak compared to electrochemical fields ($>10^9\,V\,m^{-1}$), and are comparable to those around ions in solution. The first voltage drop moves to much lower temperatures as the strength is increased: the D-defect drift velocity is not simply proportional to field strength. The field must lower the activation barrier for motion. The first-drop temperatures from Fig. 3 are plotted against field strength in Fig. 4; four points fall on a line. The fifth point corresponds to the highest field, which probably permitted ion motion *during* ion deposition. The zero-field limit is 124 K, in agreement with previous work for mobilization of pre-existing defects[22]. The D-defect mobility temperature falls to 0 K at an extrapolated field of $16 \times 10^7\,V\,m^{-1}$. This is the field at 17 Å from a singly charged ion in water, before solvation via reorientation occurs ($\epsilon = 3.2$). Thus an ion may be able to induce rapid D-defect migration as far away as 17 Å, greatly facilitating its solvation. Theoretical estimates of this field effect do not to our knowledge exist[23].

The work reported here suggests the need to refine the physical model of water ice. □

Received 19 October 1998; accepted 20 January 1999.

1. Hobbs, P. V. *Ice Physics* (Clarendon, Oxford, 1974).
2. Whalley, E., Jones, S. J. & Gold, L. W. (eds) *Physics and Chemistry of Ice* (Royal Soc. Canada, Ottawa, 1973).
3. Pomes, R. & Roux, B. Structure and dynamics of a proton wire: A theoretical study of H⁺ translocation along the single-file water chain in the gramicidin A channel. *Biophys. J.* **71**, 19–39 (1996).
4. Bainco, R., Gertner, B. J. & Hynes, J. T. Proton transfer reactions at the surface of ice. Heterogeneous reactions involved in stratospheric ozone deletion. *Ber. Bunsenges. Phys. Chem.* **102**, 518–526 (1998).
5. Eckener, U., Helmreich, D. & Engelhardt, H. in *Physics and Chemistry of Ice* (eds Whalley, E., Jones S. J. & Gold, L. W.) 242–245 (Royal Soc. Canada, Ottawa, 1973).
6. Petrenko, V. F. & Maeno, N. Ice field transistor. *J. de Phys. C* **48**, 115–119 (1987).
7. Petrenko, V. F. *Electrical Properties of Ice* (Spec. Rep. 93-20, US Army Cold Regions Research and Engineering Laboratory, Hanover, NH, 1993).
8. Collier, W. B., Ritzhaupt, G. & Devlin, J. P. Spectroscopically evaluated rates and energies for proton transfer and Bjerrum defect migration in cubic ice. *J. Phys. Chem.* **88**, 363–368 (1984).
9. Wooldridge, P. J. & Devlin, J. P. Proton trapping and defect energetics in ice from FT-IR monitoring of photoinduced isotopic exchange of isolated D_2O. *J. Chem. Phys.* **88**, 3086–3091 (1988).
10. von Hipple, A., Runck, A. H. & Westphal, W. B. in *Physics and Chemistry of Ice* (eds Whalley, E., Jones, S. J. & Gold, L. W.) 236–241 (Royal Soc. Canada, Ottawa, 1973).
11. Tsekouras, A. A., Iedema, M. J., Ellison, G. B. & Cowin, J. P. Soft-landed ions: a route to ionic solution studies. *Int. J. Mass Spectrom. Ion Proc.* **174**, 219–230 (1998).
12. Kleyn, A. W. *Ion-surface interactions—from channelling to soft-landing. Science* **275**, 1440–1441 (1997).
13. Miller, S. A., Luo, H., Pachuta, S. J. & Cooks, R. G. Soft-landing of polyatomic ions at fluorinated self-assembled monolayer surfaces. *Science* **275**, 1447–1450 (1997).
14. Engelhardt, H. in *Physics and Chemistry of Ice* (eds Whalley, E., Jones, S. J. & Gold, L. W.) 226–235 (Royal Soc. Canada, Ottawa, 1973).
15. Pfeifer, R. & Hertz, H. G. Activation energies of the proton-exchange reactions in water measured with the 1H-NMR spin echo technique. *Ber. Bunsenges. Phys. Chem.* **94**, 1349–1355 (1990).
16. Strongin, D. R., Mowlem, J. K., Lynne, K. G. & Kong, Y. Efficient magnetic focusing of low-energy ions (1–5 eV) onto solids for use in surface chemistry studies. *Rev. Sci. Instrum.* **63**, 175–188 (1992).
17. Tsekouras, A. A., Iedema, M. J. & Cowin, J. P. Soft-landed ion diffusion studies on vapor-deposited hexane films. *J. Phys. Chem.* (submitted).
18. The KP5000 system (McAllister Technical Services, Coer d'Alene, Idaho 83815, USA).
19. Materer, N. *et al.* Molecular surface structure of ice (0001): dynamical low-energy electron diffraction, total-energy calculations and molecular dynamics simulation. *Surf. Sci.* **381**, 190–210 (1997).
20. Tuckerman, M., Laasonen, K., Sprik, M. & Parrinello, M. *Ab initio* molecular dynamics simulation of the solvation and transport of hydronium and hydroxyl ions in water. *J. Chem. Phys.* **103**, 150–161 (1995).
21. Kunst, M. & Warman, J. M. Nanosecond time-resolved conductivity studies of pulse ionized ice. 2. The mobility and trapping of protons. *J. Phys. Chem.* **87**, 4093–4095 (1983).
22. Johari, G. P. & Jones, S. J. Study of the low-temperature "transition" in ice I h by thermally stimulated depolarization measurements. *J. Chem. Phys.* **62**, 4213–4223 (1975).
23. Hermansson, K. & Olamae, L. On the role of electric fields for proton transfer in water. *Solid State Ionics* **77**, 34–42 (1995).

Supplementary Information is available on *Nature*'s World-Wide Web site (http://www.nature.com) or as paper copy from the London editorial office of *Nature*.

Acknowledgements. We thank S. E. Barlow for advice. This work was conducted in the Environmental Molecular Sciences Laboratory, a collaborative users' facility of the US Department of Energy (DOE), under the Office of Biological and Environmental Research, and was supported by the Division of Chemical Sciences, US DOE. Pacific Northwest National Laboratory is operated by Battelle Memorial Institute for the US DOE.

Correspondence and requests for materials should be addressed to J.P.C. (e-mail: jp.cowin@pnl.gov).

Electrical conduction through DNA molecules

Hans-Werner Fink & Christian Schönenberger

Institute of Physics, University of Basel, Klingelbergstrasse 82, CH-4056 Basel, Switzerland

The question of whether DNA is able to transport electrons has attracted much interest, particularly as this ability may play a role as a repair mechanism after radiation damage to the DNA helix[1]. Experiments addressing DNA conductivity have involved a large number of DNA strands doped with intercalated donor and acceptor molecules, and the conductivity has been assessed from electron transfer rates as a function of the distance between the donor and acceptor sites[2,3]. But the experimental results remain contradictory, as do theoretical predictions[4]. Here we report direct measurements of electrical current as a function of the potential applied across a few DNA molecules associated into single ropes at least 600 nm long, which indicate efficient conduction through the ropes. We find that the resistivity values derived from these measurements are comparable to those of conducting polymers, and indicate that DNA transports electrical current as efficiently as a good semiconductor. This property, and the fact that DNA molecules of specific composition ranging in length from just a few nucleotides to chains several tens of micrometres long can be routinely prepared, makes DNA ideally suited for the construction of mesoscopic electronic devices.

The physical meaning of conductivity implies that there are free charge carriers available that can move under ordinary thermal conditions. This quantity is not directly accessible from measurements of the transfer rates of injected hot electrons. The simplest

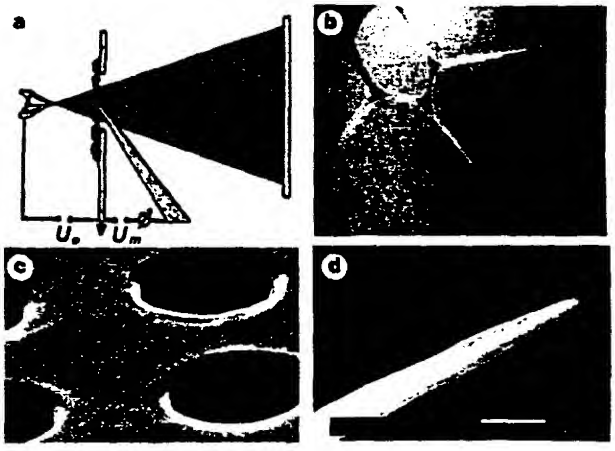

Figure 1 The low-energy electron point source (LEEPS) microscope used to investigate the conductivity of DNA. **a**, The atomic-size electron point source is placed close to a sample holder with holes spanned by DNA molecules. Due to the sharpness of the source and its closeness to the sample, a small voltage U_e (20–300 V) is sufficient to create a spherical low-energy electron wave. The projection image created by the low-energy electrons is observed at a distant detector. Between sample holder and detector, a manipulation-tip is incorporated (see text for details). This tip is placed at an electrical potential U_m with respect to the grounded sample holder and is used to mechanically and electrically manipulate the DNA ropes that are stretched over the holes in the sample holder. **b**, A projection image of λ-DNA ropes spanning a 2-μm-diameter hole. The kinetic energy of the imaging electrons is 70 eV. **c**, SEM image, showing the sample support with its 2-μm-diameter holes. **d**, SEM image of the end of a tungsten manipulation-tip used to contact the DNA ropes. Scale bar, 200 nm.

and most direct way to address the question of DNA conductivity is to arrange for a small potential difference between two well separated parts of the molecule and measure the resultant electrical current. Apart from the two contacts, the molecule should not be in contact with an object, but should instead be surrounded by vacuum to eliminate possible artefacts due to current paths other than those through the molecule itself. We have realized such an experiment by employing a modified low-energy electron point source (LEEPS) microscope[5] (Fig. 1a). An earlier study involving mechanical and electrical manipulations of carbon nanotubes[6] demonstrated the usefulness of the LEEPS technology for probing elongated molecular objects, which are placed over holes in a suitable sample holder. An electron point source provides a low-energy coherent electron beam. Thus, in a simple projection set-up, we are able to image native DNA molecules. The low energy of the imaging electrons, between 20 and 300 eV, provides high-contrast images and the absence of radiation damage[7]. The instrument is incorporated into a stainless-steel ultrahigh-vacuum chamber which provides an oil-free vacuum environment of 10^{-7} mbar. The λ-DNA molecules are placed onto a regular array of 2-μm holes in a carbon foil (Quantifoil, Jena, Germany). For a better electrical contact to the molecules, the sample holder has been covered with a gold layer. A scanning electron microscope (SEM) image of this sample holder is shown in Fig. 1c. The deposition of the molecules is achieved by first placing a drop of water containing 0.3 μg ml^{-1} of λ-DNA onto the sample holder, and then touching a piece of blotting paper to the rim of the drop to remove most of the liquid solution. (λ-DNA solution—250 μg ml^{-1}, with 10 mM Tris-HCl and 1 mM EDTA at pH 8.0 (Mannheim Boehringer)—was diluted by a factor of 1,000 with deionized water, with a resistivity of 18 MΩ cm at 25 C.) This preparation technique leads only very occasionally to individual DNA molecules spanning the holes of the sample holder: the λ-DNA usually forms networks within the holes (Fig. 1b), which implies that the DNA strands consist of a few molecules associated into a rope. If we use higher (lower) DNA concentration in solution, more (less) holes are covered by ropes while a solution containing no DNA results in no objects stretching over the holes. Due to the coherence of the electron point source, the projection images are in fact in-line holograms. In the rare case of observing a single DNA molecule stretching over a hole, the

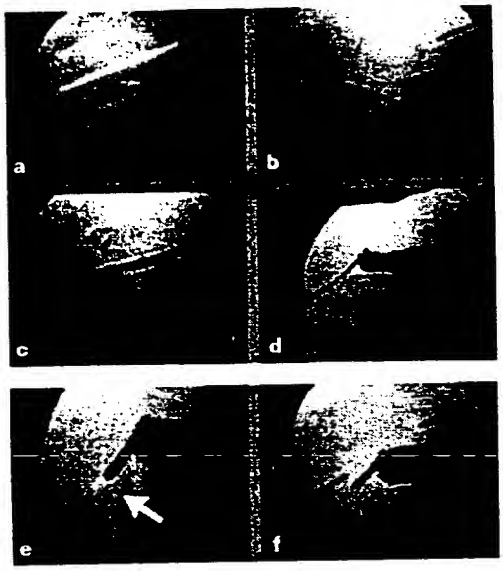

Figure 2 A sequence of LEEPS images taken with 70-eV electrons, showing the mechanical and electrical manipulation of DNA ropes. **a**, A 2-μm hole in the sample holder is selected that is spanned by just one individual DNA rope. It exhibits a length of 1.5 μm. The widening of the rope near the edge of the hole is probably due to capillary forces during evaporation of the solvent. At the surface the DNA molecules bind to the substrate and form a two-dimensional network; near the hole edges, a transition to the more compact three-dimensional rope spanning the hole is visible. Also apparent is the shadow image of the manipulation-tip that is imaged simultaneously, albeit at a low magnification as it is still at a macroscopic distance from the sample plane. Distances are measured by applying a step voltage to the piezo-ceramics on which the electron point source is mounted. This results in a lateral shift of the image corresponding to a distance given by the calibrated displacement of the piezo-ceramics. **b**, After the manipulation-tip has been moved onto the sample plane it is used to break the DNA rope into two parts. A 600-nm-long part attached to the left side of the sample holder has been bent down in order to probe its electrical conductivity by applying a voltage ramp to the manipulation-tip. Note that the magnification compared to the previous image is increased here, and only the very end of the longer (900-nm) DNA rope is apparent at the right part of the image. **c**, Further downwards motion of the manipulation-tip causes the 600-nm-long DNA piece to lose contact with the tip and flip back close to the position where it had originally been broken. **d**, An upward motion of the manipulation-tip results in a connection to both DNA ropes that now form two resistors in parallel. **e**, Extended bending and stretching of the 600-nm-long DNA rope results eventually in a defect. In contrast to the intact DNA rope, a voltage of 50 mV applied to the manipulation-tip manifests itself now (see pointer) in a potential drop along the DNA rope indicating poor conductivity at the defective region. **f**, Further mechanical stress applied to the defective DNA rope causes it to break, leaving a piece attached to the manipulation-tip.

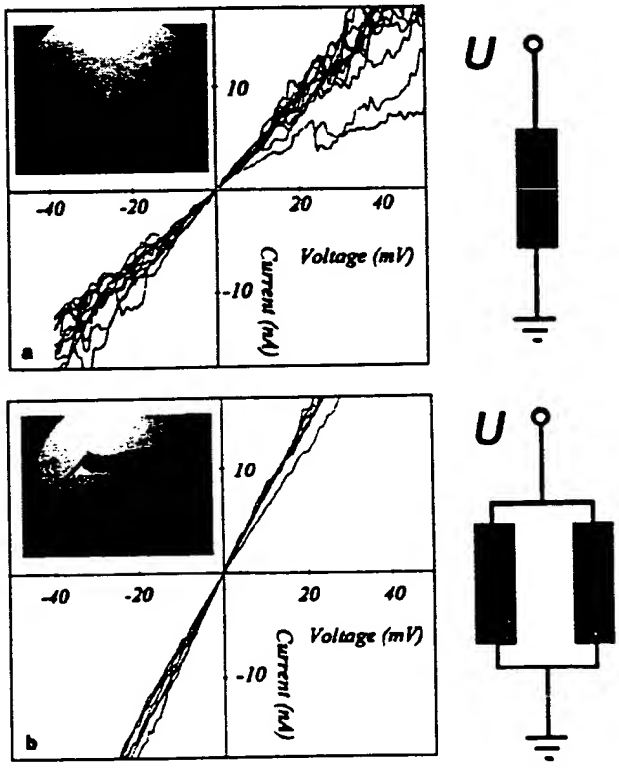

Figure 3 *I–V* characteristics of DNA ropes. **a**, *I–V* curve taken for a 600-nm-long DNA rope. In the range of ±20 mV, the curves are linear; above this voltage, large fluctuations are apparent. From the linear dependence at low voltage we derive a resistance of about 2.5 MΩ. **b**, *I–V* curve when the manipulation-tip is attached to both DNA ropes. The measured resistance drops to 1.4 MΩ. The longer DNA rope is 900 nm long, but due to the narrow angle it forms with the shank of the manipulation-tip, it is difficult to judge the actual position of the contact. Nevertheless, it appears that the situation can be viewed as a parallel connection of two resistances, 2.5 MΩ for the 600-nm rope and 3.3 MΩ for the 900-nm rope, accounting for the measured value.

reconstruction of the holograms reveals the shape of the 2-nm-wide molecule[7]. We do not observe charging effects while imaging the DNA, indicating that either the absorbed electrons are readily transported to the grounded sample holder or that no absorption of electrons takes place because all electrons are elastically scattered. We have also verified that the amount of inelastic scattered electrons is negligible. The lack of charging alone does not constitute evidence for the conductivity of the DNA. But some non-conducting objects, like small ionic crystals or latex spheres, show charging effects: the low-energy electrons are deflected by the electric fields associated with the charged objects.

Essential for the mechanical and electrical manipulation of DNA strands is the incorporation of an additional tip, the manipulation-tip (see SEM image, Fig. 1d), into the LEEPS microscope. With this additional tip, it is possible to achieve mechanical contact to a specific site of the DNA ropes, break the ropes at a certain distance from the rim of the hole in the sample holder, and place the ropes at a defined electrical potential difference with respect to the electrically grounded sample holder to which the other end of the molecules is fixed. These manipulation are performed *in situ* while the projection images of the molecules are observed on a TV monitor. In Fig. 2 we show a set of video frames illustrating the tasks necessary to probe the conductivity of DNA ropes. The circular field of view is that of the electron detector; it is not the boundary of the hole in the sample holder. First, the electron point source is moved along the hole array in the sample holder to search for a hole spanned by a single DNA rope. Once a suitable DNA rope has been identified, the manipulation-tip is moved into the field of view (Fig. 2a). The DNA molecules making up the rope and the manipulation-tip are then imaged simultaneously. As long as the manipulation-tip is still far away from the sample plane, it is imaged with a much lower magnification than the DNA rope. The tip is then moved into the sample plane to contact the DNA rope and break it into two parts. The manipulation-tip is then attached to the 600-nm-long part of the DNA rope which is forced to follow the downward motion of the tip (Fig. 2b). The conductivity of the 600-nm-long DNA rope is then probed by applying an electrical potential between the manipulation-tip and the sample holder, and monitoring the resulting current. Further downward motion of the manipulation-tip causes the DNA rope to lose contact with the manipulation-tip and to flip back close to the position where the rope had originally been broken (Fig. 2c). Next, an upward motion of the manipulation-tip causes a connection to both DNA ropes simultaneously (Fig. 2d). When an electrical potential is applied to the manipulation-tip, the resultant current can flow through either of the two DNA ropes. The projection images do not change while the applied potential is continuously varied between ± 50 mV, implying that there is no noticeable potential drop along the DNA rope. The sensitivity to small potential gradients is illustrated in Fig. 2e. The defective part of the DNA rope is clearly visible in this image, which was taken after repeated bending and stretching of the 600-nm-long DNA rope until it became defective. A negative potential applied to the manipulation-tip results in the part of the rope attached to the tip being 50 mV more negative than the grounded sample holder. This causes the low-energy electrons to be repelled, and so the projection of this part of the rope appears wider than the part attached to the grounded sample holder. With a positive voltage of the same magnitude the situation is reversed; the part attached to the sample holder appears wider. At zero bias, no effect on the image is visible. Further mechanical treatment by repeated motion of the manipulation-tip causes the DNA rope to eventually break at just this spot (Fig. 2f).

The apparent rigidity of the DNA ropes in vacuum might seem surprising, but appears to be in good agreement with standard models[8] for the elastic behaviour of the DNA. The WLC ('worm-like chain') model treats the DNA as an elastic rod. The local elastic energy is proportional to the square of the curvature, which implies that the lowest energy is associated with a rigid molecule. However, as the DNA is in solution, there will be an interplay between brownian motion and rigidity, which determines the persistence length over which the directionality of the molecule is maintained. In a vacuum environment, no brownian motion occurs, resulting in a minimal elastic energy for a molecule in a straight configuration. In a vacuum, the only external force acting on the DNA molecules is gravitation, which is extremely small for nanometre-sized objects.

We have measured current versus voltage (I–V) characteristics of the DNA ropes to obtain upper values for their resistivity. The voltage applied to the manipulation-tip is continuously swept and the current is monitored with an electrometer. These currents must be attributed to current through the molecules as they are in a vacuum: there is no alternative current path from the manipulation-tip to the grounded sample holder. Once the contact between manipulation-tip and the DNA rope is broken, the current drops to zero, confirming that no external artificial currents reach the electrometer. Also, the measured I–V characteristics do not depend on whether the situation is observed in the LEEPS microscope or not, indicating that the number of absorbed imaging electrons per second is below the noise level of the electrometer used to measure the current through the molecules. The I–V characteristics presented in Fig. 3 correspond to the situations shown in Fig. 2b and d. For the 600-nm-long DNA rope, we derive a resistance from the linear part of the I–V curve of 2.5 MΩ (Fig. 3a). If we assume that the DNA 'wire', which is made up of a few molecules, has a diameter of the same order of magnitude as that of a DNA double strand, (2 nm), we arrive at a resistivity of the order of 1 mΩ cm. This value includes a contribution due to a finite contact resistance and therefore constitutes an upper limit; the resistivity attributed to the DNA rope alone will be smaller.

The I–V curve presented in Fig. 3b corresponds to the situation where the manipulation-tip is in contact with both DNA ropes, which act as resistors in parallel. The overall resistance drops to 1.4 MΩ, implying that the longer DNA rope has a resistance of 3.3 MΩ. Again, these values have to be considered as upper limits, due to the unknown contact resistances to the metallic reservoirs. The fact that we do not observe a potential drop along the DNA molecules, as discussed above, might possibly suggest that the electrical transport through the molecules is ballistic over large distances. The linearity of the measured I–V curves around the zero point implies that we observe an equilibrium property; that is, the measured current does not stem from the injection of hot electrons into the molecules.

Although our experiments establish that DNA molecules are molecular conductors, the mechanism allowing the transport of charges remains unclear. Ionic conduction can be ruled out as the water used to dissolve and subsequently deposit the DNA molecules evaporates or sublimates long before the vacuum environment (with a base pressure of 10^{-7} mbar) has been reached and the experiment has started. Moreover, an ionic conduction mechanism would require mobile ions, such as in a liquid or a molten phase, and macroscopic ion reservoirs to maintain the stable current we observe for as long as we keep the voltage applied. Neither of the two requirements is fulfilled in our experiments; there is no liquid water phase in the vacuum and no reservoirs supplying ions. Thus the intrinsic conduction mechanism must be of an electronic nature.

Although there is no solvent water left, the presence of tightly bound water, Tris-HCl and/or EDTA molecules (and possibly also counterions attached to the DNA) cannot be ruled out, even in a vacuum environment. While the electron transport mechanism must be of an electronic nature, any molecule attached to the DNA by an ionic or covalent bond might in principle affect the electronic structure, and hence the conductivity of the DNA molecules. Even if the inner π-electrons of the base stack are responsible for carrying the current, electric patch fields due to an 'outside' ionic bond may influence the π-electron states. There are

other factors that might influence DNA conductivity. For example, if vibrational modes of the molecules participate in the conduction mechanism, a certain length of the molecule may simply be required to allow for those collective effects, like solitons, to build up and to mediate electron transport. This would imply that restrictions of the degree of freedom of the DNA molecules such as through adsorption to a surface for example, could affect electrical conduction. There are probably a range of other issues that need to be considered to understand the details of the conduction mechanism on a molecular scale, but they do not affect our finding that DNA molecules, under the conditions described here, are electrical conductors. Further carefully designed experiments are now needed to explore the factors influencing DNA conductivity. Measurements of the temperature dependence of DNA resistivity, as well as the characterization of the electrical noise, should help to determine how DNA transports charges.

The detailed understanding of the conduction mechanism remains a challenge and, once achieved, should undoubtedly provide a better insight into the biological, chemical and physical properties of DNA molecules. The work reported here suggests that DNA molecules should be considered, among other candidates, as potential one-dimensional quantum wires for mesoscopic devices. □

Received 20 May 1998; accepted 20 January 1999.

1. Dandliker, P. J., Holmlin, R. E. & Barton, J. K. Oxidative thymine dimer repair in the DNA helix. *Science* 257, 1465–1468 (1997).
2. Arkin, M. R. *et al.* Rates of DNA-mediated electron transfer between metallointercalators. *Science* 273, 475–480 (1996).
3. Lewis, F. D. *et al.* Distance-dependent electron transfer in DNA hairpins. *Science* 277, 673–676 (1997).
4. Beratan, D. N., Priyadarshy, S. & Risser, S. M. DNA: [illegible]ator or wire? *Chem. Biol.* 4, 3–8 (1997).
5. Fink, H.-W., Stocker, W. & Schmid, H. Holography with low energy electrons. *Phys. Rev. Lett.* 65, 1204–1206 (1990).
6. Schmid, H. & Fink, H.-W. Carbon nanotubes are coherent electron sources. *Appl. Phys. Lett.* 70, 2679–2680 (1997).
7. Fink, H.-W., Schmid, H., Ermantraut, E. & Schulz, T. Electron holography of individual DNA molecules. *J. Opt. Soc. Am. A* 14, 2168–2172 (1997).
8. Austin, R. H. Stretch genes. *Phys. Today* 32–38 (February 1997).

Acknowledgements. We thank our colleagues for discussions; G. Ehrlich for comments on the manuscript; and E. Ermantraut and K. Wohlfart for the design and production of the Quantifoil sample holders. This work was supported by the Swiss National Science Foundation and the Swiss priority program MINAST.

Correspondence and requests for materials should be addressed to H.-W.F. (e-mail: finkhw@ubaclu.unibas.ch).

Glacial–interglacial changes in ocean surface conditions in the Southern Hemisphere

F. Vimeux*, V. Masson*, J. Jouzel*, M. Stievenard* & J. R. Petit†

* *Laboratoire des Sciences du Climat et de l'Environnement (UMR CEA/CNRS 1572), L'Orme des Merisiers, Bâtiment 709, CEA Saclay, 91191 Gif-sur-Yvette cédex, France*

† *Laboratoire de Glaciologie et de Géophysique de l'Environnement (CNRS), 54 rue Molière, Domaine Universitaire, BP 96, 38402 St-Martin d'Hères cédex, France*

The stable-isotope signatures of oxygen and hydrogen in the water of preserved ice and snow are both widely used to infer local temperatures of past environments. A derived quantity based on these two signatures, the 'deuterium excess'[1], provides additional palaeoclimatic information[2–4], as this parameter depends on the meteorological and oceanic characteristics of the water's source-regions (in particular, their temperature[2,3] and relative humidity[4]). Published studies mainly focus on records from the past 40,000 years. Here we present a deuterium-excess history obtained from ice cores from Vostok, East Antarctica, spanning the full glacial–interglacial cycle of the past 150,000 years. The deuterium-excess record shows a strong anticorrelation with the Earth's orbital obliquity (41,000-year periodicity), and values are markedly higher during the cold stage 5d (following the last interglacial) than during the other cold stages. We interpret the relationship with obliquity as resulting from changes in the latitudinal insolation gradient affecting ocean surface conditions and, thus, the delivery of moisture to the polar region. We argue that the high 5d values, relative to other cold stages, are driven by relatively less moisture delivered from high latitudes, and more from low latitudes. The deuterium-excess in Antarctic precipitation thus provides long-term, spatially integrated information on ocean surface conditions and ocean/atmosphere circulations in the Southern Hemisphere.

The deuterium excess, *d*, (hereafter the excess) is defined as the deviation from the meteoric water line[5]: $d = \delta D - 8\delta^{18}O$ (see Fig. 1

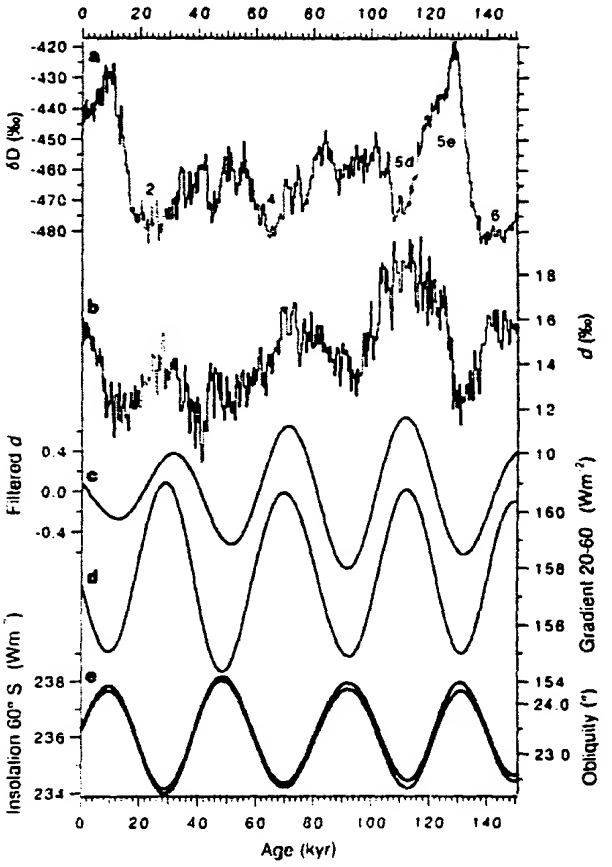

Figure 1 Time series of δD, deuterium excess, obliquity and insolation. **a**, δD; **b**, deuterium excess, *d*. Measurements were performed along a shallow core from the surface to 138 m (BH8, drilled in 1996) and along deep core 3G from 138 to 2,083 m, with different sampling resolutions (50 cm between 0 and 138 m; 5 m down to 1413 m, 2 m below this[10]). Experimental accuracy for deuterium excess is ±0.7‰ (±0.5‰ for δD and ±0.05‰ for $\delta^{18}O$) down to 1,413 m and ±1.3‰ below this ($\delta^{18}O$ measurements were performed with a dual mass spectrometer with a precision of ±0.1‰). Data are presented at a 5-m depth resolution representing a temporal resolution of 200 to 500 years. We use a modified version of the extended glaciological timescale, the accuracy of which is estimated to be ±6 kyr (ref. 10). **c**, Gaussian-filtered deuterium excess in the obliquity band (0.025 ± 0.005 kyr^{-1}). **d**, Difference between mean annual insolation at 20 S and 60 S. **e**, Mean annual insolation at 60 S (black line), and obliquity[14] (red line). (Here $\delta D = ([(D/H)_{sample}/(D/H)_{vsmow}] - 1) \times 10^3$; $\delta^{18}O = ([(^{18}O/^{16}O)_{sample}/(^{18}O/^{16}O)_{vsmow}] - 1) \times 10^3$.)